A Coherence-Based Technique to Separate and Quantify Sources of Image Degradation *in vivo* with Application to Transcranial Imaging

Emelina Vienneau, Kathryn Ozgun, and Brett Byram
Department of Biomedical Engineering
Vanderbilt University
Nashville, TN, USA
emelina.p.vienneau@vanderbilt.edu

***Abstract*—Thermal noise and acoustic clutter both impede robust transcranial ultrasound imaging, leading to difficulties in clinical translation. Currently it is not known which one is a more significant contributor to image degradation because there is no good way to separately measure their contributions *in vivo*. In this work we derive and validate a coherence-based approach for quantifying the individual contributions of thermal noise and acoustic clutter to image degradation and apply it to *in vivo* transcranial imaging of five subjects.**

I. Introduction

Transcranial ultrasound imaging is not widely used in the clinic due to poor image quality in non-neonatal patients. The high acoustic impedance mismatch between the skull and surrounding tissue leads to unacceptably low acoustic penetration and therefore signal-to-noise ratio. Other sources of image degradation such as reverberation, off-axis scattering, and phase aberration also contribute to low image quality. Although both thermal noise and acoustic clutter contribute to image degradation in transcranial ultrasound, it is not known which one is more significant because there is currently no good way to separately measure their contributions *in vivo*.

Temporal correlation is often used to compute an SNR that reflects the contributions of thermal noise, but it is unable to distinguish between clutter and tissue signal [1], [2]. Another approach to estimating thermal noise involves acquiring a "noise frame" with no prior ultrasonic transmission, but again this approach does not address acoustic clutter [3]. More recently, aperture domain techniques that leverage the coherence properties of acoustic backscatter have been used to assess sources of image degradation. These methods are sensitive to thermal noise and most types of acoustic clutter, including reverberation and off-axis scattering, but do not fully characterize the relative contribution of each source of degradation [4], [5]. Clever simulation approaches and well-designed phantom experiments can accomplish this task by imaging a medium with and without a layer of material (such as an abdominal wall) that causes reverberation and phase aberration, but this cannot be performed *in vivo* [6], [7]. Currently, the standard technique to assess clutter *in vivo* requires measuring signal power within a large anechoic or hypoechoic region such as the bladder, a large fluid-filled cyst, or a large blood vessel [8]. This will suffice if such a region can be manually identified, but that is not always the case in many clinical imaging scenarios. Furthermore, this measurement of clutter only provides information about clutter at that particular depth or region of the image rather than throughout the entire field of view. This makes it difficult to understand the spatial distribution of clutter in a given imaging scenario. Recently another technique based on spatial coherence was developed to measure incoherent noise and phase aberration, but this approach groups thermal noise with incoherent clutter rather than separating them [9]. Herein, we present a technique to separately measure the thermal noise power and the acoustic clutter power *in vivo*.

II. Methods

A. Coherence of Speckle, Noise, and Clutter

According to the van Cittert-Zernike (VCZ) theorem, the spatial (aperture domain) coherence of speckle measured with a rectangular aperture can be modeled by a triangle function, $\Lambda[m/M]$, where *m* is the channel number or lag and *M* is the total number of channels used for transmit focusing [10]–[12]. Spatial coherence of thermal noise is a delta function since thermal noise is uncorrelated [2]. Practically, the measured spatial coherence of noise will only approximate a delta function due to the finite nature of the aperture. Sources of acoustic clutter such as reverberation, some off-axis scattering, and high frequency phase aberration have also been shown to exhibit rapid decorrelation across the aperture, producing an approximate delta function as well [13].

The acoustic signal measured by the transducer during an *in vivo* image acquisition, denoted by y, will be a combination of the uncorrupted tissue signal, thermal noise, and acoustic clutter. Assuming the signals are all uncorrelated, the combined spatial coherence of such a signal is given by Eqn. (1), where P_s, P_n, and P_c are the power of the tissue, noise, and clutter, respectively [2], [13], [14].

$$\hat{R}_y[m] \propto \Lambda[m/M] + \frac{P_n}{P_s}\delta[m] + \frac{P_c}{P_s}\delta[m] \tag{1}$$

978-1-7281-5448-0/20/$31.00 ©2020 IEEE

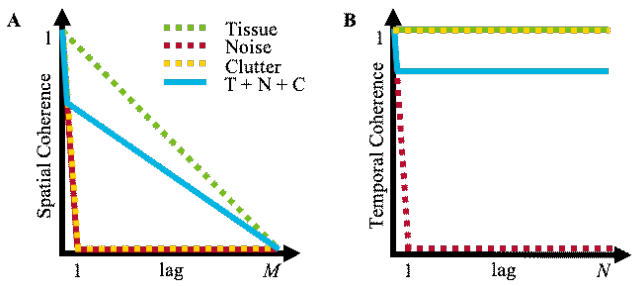

Fig. 1. Theoretical coherence curves for signal components across the aperture dimension (A) and the temporal dimension (B).

Equation (1) implies that the spatial coherence curve will have a drop at lag one proportional to the combined noise and clutter power. The lag-one coherence (LOC) therefore encapsulates the total power of the thermal noise and incoherent acoustic clutter [2], [4], [15]. The theoretical spatial coherence of the tissue, noise, and clutter components and their superposition is shown in Fig. 1A.

Across the slow-time or ensemble dimension, stationary tissue signal is coherent since speckle is deterministic. In addition, acoustic clutter is also deterministic, making tissue and clutter indistinguishable in this dimension [13], [16]. However, thermal noise is uncorrelated and can be modeled as a delta function. The temporal LOC therefore encapsulates the thermal noise power only. The theoretical temporal coherence of the tissue, noise, and clutter components and their superposition is shown in Fig. 1B.

B. Solving for Speckle, Noise, and Clutter Power

Solving for the individual speckle (uncorrupted on-axis echoes), noise, and clutter powers enables the calculation of true signal-to-noise (SNR) and signal-to-clutter (SCR) ratios, where SNR represents the contribution of thermal noise only and SCR represents the contribution of acoustic clutter only. The following sections explain the procedure for estimating these values.

1) Compute Channel and Temporal LOC: The first step is to calculate the temporal and channel LOC values from the data. The channel LOC is calculated according to Eqn. (2) for all lag-one channel pairs, a and b, and for all observations within the axial window from k_1 to k_2. The symbol * indicates the complex conjugate.

$$\rho_{\text{chan}} = \frac{\sum_{k=k_1}^{k_2} a_k b_k^*}{\sqrt{\sum_{k=k_1}^{k_2} a_k a_k^* \sum_{k=k_1}^{k_2} b_k b_k^*}} \tag{2}$$

The temporal LOC can be calculated according to Eqn. (3). Note that this is still computed on the delayed channel data to facilitate comparison with channel LOC.

$$\rho_{\text{time}} = \frac{\sum_{k=k_1}^{k_2} a_k b_k^*}{\sqrt{\sum_{k=k_1}^{k_2} a_k a_k^* \sum_{k=k_1}^{k_2} b_k b_k^*}} \tag{3}$$

2) Compute Channel and Temporal SNR from LOC Values: The channel SNR can then be written in terms of the channel LOC [4]:

$$\text{SNR}_{\text{chan}} = \frac{\rho_{\text{chan}}}{1 - \frac{1}{M} - \rho_{\text{chan}}} \tag{4}$$

Likewise, the temporal SNR can be written in terms of the temporal LOC [1]:

$$\text{SNR}_{\text{time}} = \frac{\rho_{\text{time}}}{1 - \rho_{\text{time}}} \tag{5}$$

3) Compute the total power of the channel data: The observed signal (y) is the sum of the speckle (s), the noise (n), and the acoustic clutter (c) and can be written according to Eqn. (6).

$$y = s + n + c \tag{6}$$

Assuming that the speckle, noise, and clutter signals are uncorrelated [13], the power of the observed signal, P_y, can be written as:

$$P_y = P_s + P_n + P_c \tag{7}$$

P_y can be estimated directly by computing the power of the channel data.

4) Solve for the Speckle, Noise, and Clutter Powers: From observations in Section II-A, we can further write channel SNR and temporal SNR in terms of tissue, noise, and clutter power:

$$\text{SNR}_{\text{chan}} = \frac{P_s}{P_n + P_c}. \tag{8}$$

$$\text{SNR}_{\text{time}} = \frac{P_s + P_c}{P_n}. \tag{9}$$

Together, Eqns. (4), (8), (5), and (9) relate the spatial LOC and the temporal LOC to the tissue, noise, and clutter power. Equations (7), (8), and (9) can be algebraically manipulated to solve for the three unknowns: tissue power (P_s), clutter power (P_c), and noise power (P_n):

$$P_s = \frac{\text{SNR}_{\text{chan}} P_y}{\text{SNR}_{\text{chan}} + 1} \tag{10}$$

$$P_c = \frac{P_y \text{SNR}_{\text{time}} - P_s(\text{SNR}_{\text{chan}} + 1)}{(\text{SNR}_{\text{time}} + 1)(\text{SNR}_{\text{chan}} + 1)} \tag{11}$$

$$P_n = P_y - P_s - P_c \tag{12}$$

5) Calculate True SNR, True SCR, and SCNR: Once P_s, P_c, and P_n are solved for, the signal-to-thermal-noise ratio (13), signal-to-clutter ratio (14), and signal-to-clutter-plus-noise ratio (15) can be calculated.

$$\text{SNR} = 10\log_{10}\left(\frac{P_s}{P_n}\right) \tag{13}$$

$$\text{SCR} = 10\log_{10}\left(\frac{P_s}{P_c}\right) \tag{14}$$

$$\text{SCNR} = 10\log_{10}\left(\frac{P_s}{P_n + P_c}\right) \tag{15}$$

Note that Eqn. (15) is equivalent to a spatial lag-one coherence approach to estimating channel SNR, but Eqns.

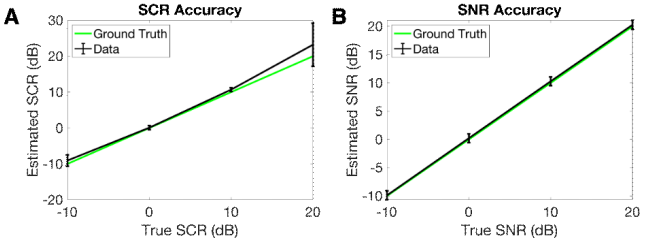

Fig. 2. SCR (A) and SNR accuracy (B) of proposed technique based on Field II simulations of 10 independent phantom realizations with varying levels of noise and clutter added. Error bars indicate mean ± SD over phantom realizations and noise levels, *i.e.* N=40 for each point.

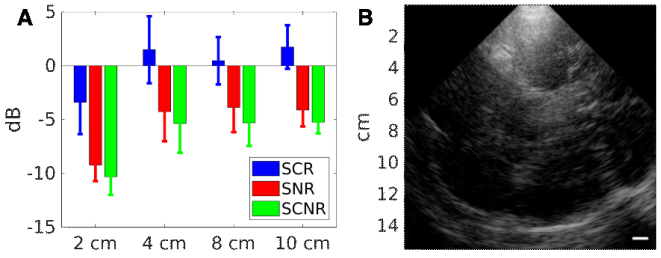

Fig. 3. (A) SCR, SNR, and SCNR measurements using the proposed technique at different depths. For each depth, only regions within the transmit focus were used for calculations. Five subjects were scanned multiple times, but the number of images that were used for analysis at 2 cm, 4 cm, 8 cm, and 10 cm was 5, 5, 20, and 4, respectively. Error bars show standard deviation. (B) Example transcranial focused B-mode image in healthy adult male subject. Dynamic range is 70 dB, scale bar is 1 cm.

(13) and (14) would be impossible to estimate without first separating the thermal noise and acoustic clutter contributions. Using Eqn. (13) and Eqn. (14), the contributions of thermal noise and acoustic clutter can be evaluated separately and compared to determine which one is a more significant cause of image degradation in any given *in vivo* imaging scenario and throughout any given field of view, assuming appropriate synthetic focusing is performed to ensure valid application of the VCZ theorem.

C. Simulations

In order to determine the accuracy of this method, simulations were conducted using Field II in MATLAB (Mathworks, Natick, Massachusetts) [17], [18]. A 64-element linear array (0.3 mm pitch, 65% fractional bandwidth) was simulated with an imaging frequency of 2.72 MHz. The transmit focal depth was 4 cm and dynamic receive beamforming with rectangular apodization was performed. Ten frames and 128 beams were acquired. The tissue phantom speed of sound was 1540 m/s and there were 16 scatterers per resolution cell. The clutter channel data were created using a previously reported pseudo-nonlinear approach to simulating reverberation with Field II [7]. Parameters were chosen as suggested by Byram *et al.* to ensure aperture domain coherence curves with near delta function appearance, thereby serving as a sufficient model of clutter [7].

After creating the tissue and clutter channel data, the noise channel data were created from samples of the standard normal distribution. Twenty independent slow-time frames were generated. To create the slow-time frames for the tissue and clutter data, the channel data were simply replicated since stationary tissue and clutter are temporally stable. The tissue, clutter, and noise channel data were then combined via coherent summation at combinations of noise-to-tissue levels and clutter-to-tissue levels ranging from -10 to 20 dB in increments of 10 dB (16 different combinations). This process was repeated for 10 independent realizations of tissue + clutter + noise phantoms. Finally, true SCR and true SNR values were estimated according to Eqns. (13) and (14). Lag-one coherence values were calculated using an axial kernel of 5λ within a 2 mm ROI centered about the transmit focus.

D. In vivo Imaging

In vivo transcranial imaging was performed at the acoustic window in five healthy adult subjects. The transducer was oriented to capture the transverse plane. For each subject, multiple acquisitions at transmit focal depths of 2 cm, 4 cm, 8 cm, and 10 cm were obtained. Imaging was performed with a 64 element P4-2v array (pitch = 0.3 mm) with 2.72 MHz imaging frequency and a Verasonics Vantage 128 ultrasound scanner. Ten slow-time frames and 128 beams were acquired. Dynamic receive beamforming and rectangular apodization were performed.

III. Results

Figure 2 shows the ability of the proposed technique to accurately measure SCR and SNR across varying levels of added noise and clutter within the range of -10 to 20 dB. Note that the signal-to-clutter-plus-noise range was -20 to 40 dB. The sum squared error between the average calculated values and the known values is 11.63 dB for SCR and 0.21 dB for SNR, indicating that this method is accurate for the range over which it was tested. It is worth noting that all underlying assumptions concerning the coherence properties of speckle, noise, and clutter were tested and satisfied in the Field II simulations, but future work should investigate the performance of this technique in physical phantom experiments. However, simulations are advantageous in that noise and clutter can be added to the tissue at precisely controlled levels, whereas in a physical phantom the true amount of noise and clutter cannot be known.

Figure 3A shows SCR, SNR, and SCNR values calculated using the proposed technique at various transmit focal depths for *in vivo* transcranial imaging of five healthy adult subjects. An example transcranial B-Mode is shown in Fig. 3B. From Fig. 3A, we see that at a 2 cm focal depth noise and clutter are both severe due to the excessive near-field reverberation from the skull and scalp. Throughout, SNR remains lower than SCR, indicating that thermal noise may be a larger contributor to image degradation than acoustic clutter in transcranial imaging. While these results are still preliminary, if validated by additional experimentation, they would indicate

that techniques to improve the thermal signal-to-noise ratio should be pursued first in order to achieve the largest benefits in transcranial ultrasound imaging.

IV. Conclusion

In summary, we have shown that our new coherence-based approach to separating and quantifying thermal and acoustic noise is accurate in Field II simulations over a reasonable range. We have also applied our technique to transcranial imaging of five healthy adult subjects. These preliminary *in vivo* results suggest that thermal noise may contribute more to image degradation than acoustic clutter in transcranial imaging, suggesting that techniques to overcome thermal noise should be pursued first.

Acknowledgment

The authors would like to acknowledge the staff at Vanderbilt University's Advanced Computing Center for Research and Education (ACCRE) for their continued support. This work has been supported by the award T32EB021937 from the National Institutes of Health as well as the award IIS-1750994 from the National Science Foundation.

References

[1] B. H. Friemel, L. N. Bohs, K. R. Nightingale, and G. E. Trahey, "Speckle decorrelation due to two-dimensional flow gradients," *IEEE Transactions on Ultrasonics, Ferroelectrics, and Frequency Control*, vol. 45, no. 2, pp. 317–327, 1998.

[2] N. B. Bottenus and G. E. Trahey, "Equivalence of time and aperture domain additive noise in ultrasound coherence," *The Journal of the Acoustical Society of America*, vol. 137, no. 1, pp. 132–138, 2015.

[3] C. Huang, P. Song, P. Gong, J. D. Trzasko, A. Manduca, and S. Chen, "Debiasing-Based Noise Suppression for Ultrafast Ultrasound Microvessel Imaging," *IEEE Transactions on Ultrasonics, Ferroelectrics, and Frequency Control*, vol. 66, no. 8, pp. 1281–1291, 2019.

[4] W. Long, N. Bottenus, and G. E. Trahey, "Lag-one coherence as a metric for ultrasonic image quality," *IEEE Transactions on Ultrasonics, Ferroelectrics, and Frequency Control*, vol. 65, no. 10, pp. 1768–1780, 2018.

[5] M. R. Morgan, G. E. Trahey, and W. F. Walker, "Multi-covariate Imaging of Sub-resolution Targets," *IEEE Transactions on Medical Imaging*, vol. 38, no. 7, pp. 1690–1700, 2019.

[6] G. F. Pinton, G. E. Trahey, and J. J. Dahl, "Erratum: Sources of image degradation in fundamental and harmonic ultrasound imaging: A nonlinear, full-wave, simulation study," *IEEE Transactions on Ultrasonics, Ferroelectrics, and Frequency Control*, vol. 58, no. 6, pp. 1272–1283, 2011.

[7] B. Byram and J. Shu, "Pseudononlinear ultrasound simulation approach for reverberation clutter," *Journal of Medical Imaging*, vol. 3, no. 4, p. 046005, 2016.

[8] M. A. Lediju, M. J. Pihl, J. J. Dahl, and G. E. Trahey, "Quantitative assessment of the magnitude, impact and spatial extent of ultrasonic clutter," *Ultrasonic Imaging*, vol. 30, no. 3, pp. 151–168, 2008.

[9] J. Long, W. Long, N. Bottenus, and G. Trahey, "Coherence-based quantification of acoustic clutter sources in medical ultrasound," *Journal of the Acoustical Society of America*, vol. 148, no. 2, pp. 1051–1062, 2020.

[10] Joseph W. Goodman, *Statistical Optics*. Hoboken, NJ, USA: John Wiley & Sons, 2015.

[11] R. Mallart and M. Fink, "The van Cittert-Zernike theorem in pulse echo measurements," *Journal of the Acoustical Society of America*, vol. 90, no. November, pp. 2718–2727, 1991.

[12] D. L. Liu and R. C. Waag, "About the Application of the Van Cittert-Zernike Theorem in Ultrasonic Imaging," *IEEE Transactions on Ultrasonics, Ferroelectrics, and Frequency Control*, vol. 42, no. 4, pp. 590–601, 1995.

[13] G. Pinton, G. Trahey, and J. Dahl, "Spatial coherence in human tissue: Implications for imaging and measurement," *IEEE Transactions on Ultrasonics, Ferroelectrics, and Frequency Control*, vol. 61, no. 12, pp. 1976–1987, 2014.

[14] N. Bottenus, B. C. Byram, J. J. Dahl, and G. E. Trahey, "Synthetic aperture focusing for short-lag spatial coherence imaging," *IEEE Transactions on Ultrasonics, Ferroelectrics, and Frequency Control*, vol. 60, no. 9, pp. 1816–1826, 2013.

[15] W. Long, N. Bottenus, and G. E. Trahey, "Incoherent Clutter Suppression using Lag-One Coherence," *IEEE Transactions in Ultrasonics, Ferroelectrics, and Frequency Control*, vol. 3010, no. c, pp. 1–14, 2020.

[16] J. J. Dahl and N. M. Sheth, "Reverberation clutter from subcutaneous tissue layers: Simulation and in vivo demonstrations," *Ultrasound in Medicine and Biology*, vol. 40, no. 4, pp. 714–726, 2014.

[17] J. Jensen, "A model for the propagation and scattering of ultrasound in tissue," *Journal of the Acoustical Society of America*, vol. 89, no. 1, pp. 182–190, 1991.

[18] J. A. Jensen and N. B. Svendsen, "Calculation of pressure fields from arbitrarily shaped, apodized, and excited ultrasound transducers," *IEEE Transactions on Ultrasonics, Ferroelectrics and Frequency Control*, vol. 39, no. 2, pp. 262–267, 1992.